

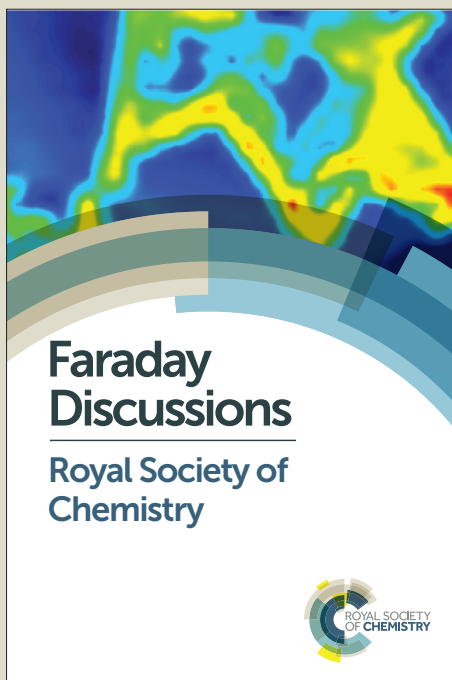
Faraday Discussions

Accepted Manuscript



This manuscript will be presented and discussed at a forthcoming Faraday Discussion meeting. All delegates can contribute to the discussion which will be included in the final volume.

Register now to attend! Full details of all upcoming meetings: <http://rsc.li/fd-upcoming-meetings>



This is an *Accepted Manuscript*, which has been through the Royal Society of Chemistry peer review process and has been accepted for publication.

Accepted Manuscripts are published online shortly after acceptance, before technical editing, formatting and proof reading. Using this free service, authors can make their results available to the community, in citable form, before we publish the edited article. We will replace this *Accepted Manuscript* with the edited and formatted *Advance Article* as soon as it is available.

You can find more information about *Accepted Manuscripts* in the [Information for Authors](#).

Please note that technical editing may introduce minor changes to the text and/or graphics, which may alter content. The journal's standard [Terms & Conditions](#) and the [Ethical guidelines](#) still apply. In no event shall the Royal Society of Chemistry be held responsible for any errors or omissions in this *Accepted Manuscript* or any consequences arising from the use of any information it contains.

Faraday Discussion 'Single-Entity Electrochemistry'

High-bandwidth detection of short DNA in nanopipettes

Raquel Fraccari,¹ Marco Carminati,² Giacomo Piantanida,² Tina Leontidou,¹ Giorgio Ferrari,² Tim Albrecht^{1*}

¹ Imperial College London, Department of Chemistry, Exhibition Road, London SW7 2AZ, UK

² Politecnico di Milano, Dipartimento di Elettronica, Informazione e Bioingegneria, P.za Leonardo da Vinci 32, Milano, Italy

Abstract:

Glass or quartz nanopipettes find increasing use as tools for studying the biophysical properties of DNA and proteins, and as sensor devices. The ease of fabrication, favourable wetting properties and low capacitance are some of the inherent advantages, for example compared to more conventional, silicon-based nanopore chips. Recently, we have demonstrated high-bandwidth detection of double-stranded (ds) DNA with microsecond time resolution in nanopipettes, using custom-designed electronics. The electronics design has now been refined to include more sophisticated control features, such as integrated bias reversal and other features. Here, we exploit these capabilities and probe the translocation of short dsDNA in the 100 bp range, in different electrolytes. Single-stranded (ss) DNA of similar length are in use as capture probes, so label-free detection of their ds counterparts could therefore be of relevance in disease diagnostics.

Introduction

The transport of biopolymers such as DNA or RNA through nanometre-sized pores and narrow channels is a fundamental process in biology, but is of increasing technological interest, too. In nanopore sensing, for example, the process is recreated in a device consisting of an electrolyte-filled cell that is separated into two compartments by a highly insulating membrane. The latter typically features a single, or in some cases small number of, well defined pore(s) that allow for ion, liquid or analyte transport such as DNA or proteins between the two compartments. Transport across the pore may be induced by concentration, potential or pressure differences between the compartments, in accordance with the electrochemical potential gradient. Detection is typically either optical (fluorescence, SER(R)S) or electric (ion or tunnelling current),^{1,2,3,4,5} where the duration, magnitude or temporal evolution of the signal is then used to extract information about the analyte, such as length, conformation, structure or composition.^{6,7} In the latter context, prospects of fast and label-free sequencing of DNA, RNA and even proteins have inspired the field since its beginnings, with remarkable success in recent years (*vide infra*).^{8,9}

Broadly speaking, one may distinguish three classes of nanopore sensors that have been used for single-molecule detection, namely biological nanopores (> 1990s), solid-state 'chip-based' nanopore sensors (early 2000s) and nanopipettes (since ~2010). Hybrid devices aiming to combine the respective strengths have also been reported.^{10,11,12}

In biological nanopore devices, the pore is made up of a pore forming protein, such as α -hemolysin (α -HL), which is typically embedded in a lipid-bilayer membrane.³ In the case of α -HL, the channel is rather narrow, so that single-stranded (ss)DNA can pass through, but dsDNA or larger biomolecular complexes cannot. The pores are highly reproducible, in terms of size and sensor performance.

In chip-based devices, the membrane is usually made from highly insulating dielectric materials, such as SiO₂ or Si₃N₄, or two-dimensional materials such as graphene or MoS₂, and the pore is milled using a focused ion or electron beam.^{13,14,4,15} Compared to biological pores, the pore size is less reproducible, but at the same time the design more flexible, in that larger pores may be used to probe larger analytes, such as protein/DNA complexes.^{16,32} In conventional chip-based devices, Si has been used as the base material, which however exhibits rather unfavourable electric characteristics, including high capacitance and therefore high electric noise. As a consequence,

recent efforts have been directed to replacing Si by glass or quartz as the base material, with remarkable reduction in device capacitance to below 10 pF, in some cases even below 1 pF.^{17,18,19}

Finally, small micro- or nanopipettes have been used in patch clamping to probe ion transport across cell membranes since the 1970s,^{20,21} and for surface imaging in Scanning Ion Conductance Microscopy (SICM) since the late 1980s.^{22,23} Only recently have they been employed for the single-molecule detection and characterisation of DNA or proteins.^{7,24,25,42} Compared to conventional chip-based devices, advantages include ease of fabrication outside of the cleanroom, favourable wetting properties (in aqueous electrolytes) and low device capacitance (facilitating high-bandwidth electric recording). While nanopipettes with pore diameters around 20 nm can be fabricated directly using a pipette puller, making single-nm pores is difficult and typically requires post-modification, e.g. by Atomic Layer Deposition (ALD),²⁶ or electron beam-induced reshaping.²⁴ This can be desirable, for example to enhance the signal-to-noise ratio for the detection of small analytes, such as proteins.

It is difficult to characterize the shape of the pore channel on the inside of the pipette directly, and in particular close to the sensing region. However, it may be reconstructed from the current-time trace by translocating geometrically well-defined analytes, such as spherical nanoparticles.²⁷ In practice, it is often assumed that the channel is conical until the very end of the tip, with good agreement between theory and experiment.

In any case, nanopipettes now constitute a well-established platform for the study of fundamental ion- and liquid transport processes, and as a biophysical tool. In the present paper, we build on our recent work on the development of high-bandwidth low-current detection electronics and translocation of "long" DNA in kilo basepair (kbp) range. We present a revised electronic circuitry with additional features, including built-in large-amplitude bias reversal ('zapping') and fully integrated software control. We focus on the translocation of short, 100 and 200 bp dsDNA (geometric length $L_{DNA} \sim 34$ and 68 nm, respectively) in nanopipettes with pore diameters between 17 and 26 nm. The DNA lengths are thus comparable to the persistence length of dsDNA, which is on the order of 35 nm and higher (depending on the electrolyte conditions),^{28,29} and the translocating analyte more akin to a rigid rod than a flexible, long polymer. Accordingly, as we show below, we no longer find different folding states in the translocation data, which was reported previously for

dsDNA in the kbp range.^{6,7} ssDNA of similar length are also used as capture probes in disease diagnostics,³⁰ so the label-free detection of their double-stranded counterparts may find application in biomedical sensing.

Materials and Methods

DNA samples. The linear 100bp dsDNA was obtained by hybridization of two complementary ssDNA strands. For the hybridization, 100 picomole of each ssDNA strand was added to 5 μ L of PerfectHybTM Plus hybridization buffer (Sigma Aldrich, Dorset, UK) and 43 μ L of UltraPureTM DNase/RNase-Free distilled water (Life Technologies, CA, USA). The mixture was first heated at 95 $^{\circ}$ C for 5 minutes then incubated at 37 $^{\circ}$ C for five hours then finally cooled at 4 $^{\circ}$ C for 20 minutes before storing a -20 $^{\circ}$ C until use. Linear 200 bp dsDNA was purchased from Fisher Scientific (Leicestershire, UK) and stored at -20 $^{\circ}$ C until use. The DNA concentrations were measured by UV- Vis spectroscopy (NanoDrop 2000c spectrophotometer, Thermo Scientific, MA, U.S.A) and the purity of the DNA samples confirmed on a 2 % agarose gel, see SI Fig. S1.

Nanopipette fabrication. Quartz capillaries (O.D 1 mm, ID: 0.5 mm, Length 7.5 cm) were first plasma cleaned and then pulled on a laser pipette puller (P200, Sutter Instruments, Novato, USA) using one of two programs. The programme parameters were either: HEAT: 575, FILAMENT: 3, VELOCITY: 35, DELAY: 145 and PULL: 75 for the first step, then HEAT: 900, FILAMENT: 0, VELOCITY: 15, DELAY: 128 and PULL: 200 for the second step ("Programme 57") or alternatively HEAT: 700, FILAMENT: 5, VELOCITY: 35, DELAY: 150 and PULL: 75, then HEAT: 700, FILAMENT: 0, VELOCITY: 15, DELAY: 128 and PULL: 200 ("Programme 99"). Current-voltage (I-V) curves between -1 V and +1 V were used to estimate the pore conductance. Using this measured pore conductance the diameter of the nanopores were estimated using the following equation:³¹

$$d_{pore} = \frac{4Gl + \frac{\pi}{2}GD_i}{D_i\pi g(c) - \frac{\pi}{2}G} \quad (1)$$

where D_i is the inner diameter at the capillary base (0.5 mm), G the conductance of the nanocapillary, $g(c)$ the conductivity of the electrolyte (measured for 1 M KCl: 101 mS/cm; 2 M LiCl: 100.1 mS/cm; 4 M LiCl: 167 mS/cm) and l the taper length (which was either 2 or 3 mm, depending on the pulling programme used, see above).

Translocation experiments. Glass vials ($V = 2$ mL) were rinsed with 70% ethanol (EtOH) and ultrapure water then filled with 1 mL of the respective electrolyte solution (e.g. 4 M LiCl, 10 mM Tris·HCl pH 8), as indicated. The nanopipettes were backfilled with the same electrolyte as the vial and fixed to the cap. For each experiment two freshly prepared 0.25 mm Ag/AgCl electrodes were used; the counter electrode (CE) was inserted inside the nanopipette and the working electrode (WE) placed in the electrolyte solution surrounding the nanopipette. The DNA concentrations ranged from 3 nM - 6 nM and a negative bias voltage applied to the working electrode (i.e. electrophoretic transport of DNA is from the outside to the inside of the pipette).

Ionic current measurements. As discussed in more detail below, a low-noise, wide-bandwidth CMOS current amplifier was employed for the ionic current measurements.^{42,32} Briefly, the custom-built amplifier splits the measured ionic current into a slowly responding ('DC channel') that contains the open pore current of the nanopore, and a fast responding ('AC channel') where short current transients such as translocation events are displayed. For translocation experiments, the AC channel was filtered at up to 100 kHz and sampled at 1 Ms/s. The low-noise amplifier is placed inside a Faraday cage as close as possible to the nanopipette so that the parasitic capacitance of connecting wires and the coupling of interferences would be minimized.

Data analysis. The ion current transients were analyzed with a custom written MATLAB script and Origin 9.0. Translocation events were defined as current transients with a depth (or peak amplitude) I_p greater than a 4 or 5σ , as indicated (σ is the standard deviation of noise in the AC channel). The dwell time, τ was defined as the time difference between the data points where current crossed a 1σ cutoff for each event. Such a threshold was chosen to preserve the overall shape of each translocation event as much as possible, while reducing the effect of (small) local baseline fluctuations.

Results

We start with a discussion of the electronics design. A key role in the setting the ultimate performance of a nanopore sensing system is played by the current amplifier employed to measure the ionic current. The two most important features of such an amplifier are its current resolution (i.e. its noise) and its speed (i.e. its bandwidth BW). High resolution is required in order to retrieve information from the details of the pulse produced by the molecule translocation, while speed is clearly useful to achieve high throughput and to detect short molecules and fast events.

Unfortunately, these properties are strictly related and cannot be chosen independently: the higher the bandwidth, the higher the noise. Advanced circuitual topologies can be adopted in order to design novel amplifiers that partially relax this fundamental trade-off, which is extremely stringent in classical transimpedance amplifiers.³³ In any case, the minimization of the amplifier noise should represent a primary goal in the development of advanced nanopore platforms.³⁴ An important guideline to achieve this target is the minimization of the amplifier input capacitance. This capacitance is the sum of several contributions, including the capacitance of the shielded coaxial cable connecting the working electrode to the amplifier (proportional to the cable length with a specific capacitance of 50-100 pF per meter), and the stray capacitance of the device itself. Thus, an accurate design of both the sensing setup (minimization of cable length) and of the device (choice of proper materials and geometries) is crucial. In the literature, few examples demonstrate enhanced noise performances achievable by accurate device design, including the choice of glass substrates^{35,36,37} and thick isolation from the ionic solution.³⁸

One effective solution that provides significant advantages is the implementation of the current amplifier into a single microelectronic chip.³⁹ Thanks to its miniaturization (area of a few mm²), it can be placed in very close proximity of the electrodes. Furthermore, the ultimate level of connection shrinking is achievable when a metal pad (properly treated) of the chip serves as working electrode.³⁸ Finally, the straightforward integration of several amplifiers in parallel in a single chip, enables multi-channel operation.

Recently, we have presented an integrated CMOS current amplifier, specifically designed for low-capacitance nanopore applications offering unrivalled performance: DC to 3.5 MHz bandwidth, 6 pA_{rms} resolution with BW=100 kHz (i.e. the max. BW of Axopatch 200B, having twice the noise), and 50 pA_{rms} resolution with BW=1 MHz (the limit of the Chimera CMOS amplifier,⁴⁰ having twice the noise) in open circuit condition (input capacitance \approx 3.5 pF). The architecture of the amplifier leverages a self-compensating integrator-differentiator topology based on matched-MOSFETs,⁴¹ endowed with an additional feedback network for handling large DC signals (\pm 100 nA) and thus zooming with high gain (470 MV/A) on the details of the translocation signal. This amplifier allows achieving state-of-the-art speed with low-capacitance devices (ideally <1-10 pF) such as glass nanopipettes.⁴²

Here we introduce an original and complete electronic platform built around the integrated amplifier for versatile nanopore sensing. In fact, once the amplifier noise has been minimized at

best, it becomes necessary to minimize also the noise of the voltage generator used to bias the counter electrode, since it is also injected in the signal path, so contributing to the total noise. Thus, the main novelty of the current platform is to include an on-board a low-noise voltage generator along with auxiliary circuitry for versatile operation. As shown in Fig. 1, a microcontroller (Arduino DUE) drives a 16-bit DAC (AD5570) whose output is abundantly low-pass filtered (at 1 Hz). The microcontroller allows application of both a constant bias and triangular waveforms for cyclic voltammetry. A digitally-controlled precision analog switch (ADG5204, MUX in Fig. 1A) then allows applying to the counter electrode one of the four signals: (1) unfiltered DAC output for applying fast signals (such as a “zapping” transient voltage pulses to unclog the pore), (2) the filtered DAC output, (3) an inverted version of the DAC output for fast bias reversing,^{43,44} (4) an external signal such as a small sinusoidal voltage, useful for impedance measurement during the device characterization. The switch commutation time is very fast (<300 ns), thus allowing abrupt bias reversal, while preserving the low-noise quality of both low-pass-filtered and locally generated biasing potentials. A fast control logic based on selectable thresholds allows automatic reverse biasing when translocation is detected. The prototype platform of this single-board and versatile platform is extremely compact (8 cm by 8 cm, Fig. 1B). The data presented in this manuscript were detected either with this new setup or the one reported previously (*cf.* SI).⁴²

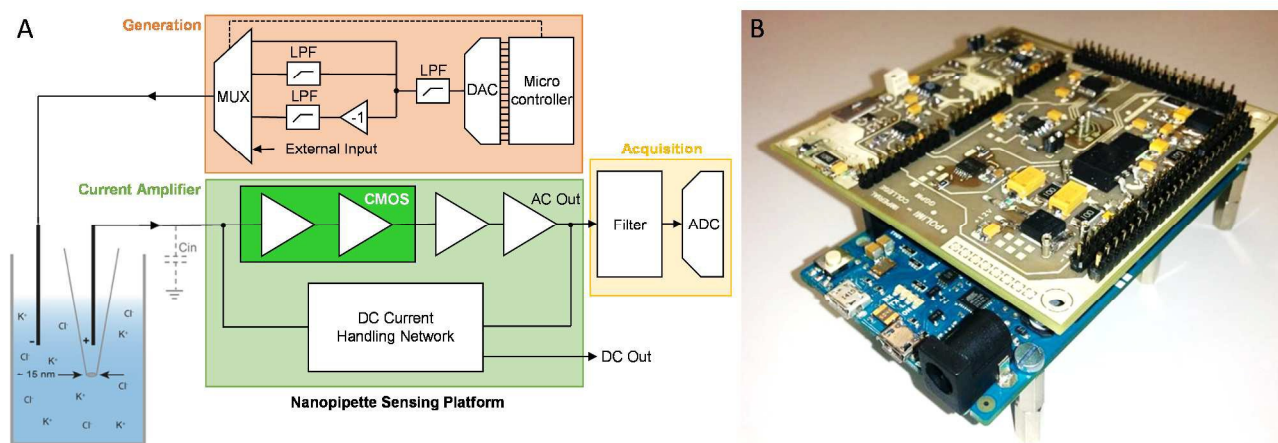


Fig 1: A) Block scheme of the dedicated nanopore characterization platform combining ultra-low-noise current reading and voltage biasing along with additional features such as zapping and automatic reverse biasing. B) Photograph of the compact prototype platform (8 cm by 8 cm), dissipating 125 mA at ± 15 V plugged onto the Arduino DUE microcontroller that is managing all the operating modes.

Based on previous data, we first estimated the minimum dsDNA length $L_{DNA,m}$ that we would be most likely to be able to detect under the conditions used here (1 M KCl electrolyte solution, similar pore diameter, filter frequency ~ 100 kHz), assuming that the scaling factor of the translocation time with DNA does not change significantly.[‡] Further details of this assessment can be found in the SI. Briefly, we first extracted the I_p values for four DNA lengths (4, 5.31, 10, and 48.5 kbp) at four different V_{bias} (-200, -300, -400, and -800 mV), as well as the AC root-mean-square (rms) noise I_{rms}^{AC} of the AC channel under the respective filter conditions (Table S1, in the SI). We found the signal-to-noise ratio (S/N) I_p/I_{rms}^{AC} to be 7.4 on average, and independent of V_{bias} and L_{DNA} (note the different filter frequencies, however). In a second step, we took the most probable translocation times τ_{mp} for each L_{DNA} and V_{bias} , and calculated the corresponding scaling law, $\log(\tau_{mp})$ vs. $p \cdot \log(L_{DNA})$. p is the scaling factor and was found to be between 1.16 and 1.24. With S/N approximately length independent, we then calculated the minimum $L_{DNA,m}$, for which $\tau = 10$ μ s, for each V_{bias} . This yielded $L_{DNA,m}$ values of 326, 480, 684 and 1152 bp for $V_{bias} = -200, -300, -400$ and -800 mV. The approximately linear dependence between $L_{DNA,m}$ and V_{bias} (Figure S4) further allowed for extrapolation to $V_{bias} = -50$ and -100 mV, yielding $L_{DNA,m} = 152$ and 220 bp. Thus, we would expect to be able to detect translocation of dsDNA in the few 100 bp range, in 1 M KCl and at low V_{bias} . Events shorter than 10 μ s might still be detected, but not fully resolved due to filter convolution. Smaller pore diameters, alternative electrolytes (such as LiCl, *vide infra*) or surface modification would potentially enable detection of even shorter DNA segments with nanopipettes.^{45,46,47}

Indeed, we were subsequently able to confirm this rather crude estimate experimentally, based on translocation experiments with 200 bp dsDNA in 1 M KCl ($V_{bias} = -300$ mV), as shown in Figure 2 (we were unsuccessful in detecting translocation of 100 bp dsDNA, data not shown). In order to differentiate noise features from actual translocation events, we analyzed the current-time trace with regards to positive and negative event polarity. While DNA translocation events result in a temporal decrease in the current (negative spikes in the AC channel), random noise is expected to

[‡] This is arguably a somewhat crude approximation, and different scaling factors between DNA length and translocation time have indeed been reported previously.⁴² The estimated values nevertheless provide a useful guideline, as we show in the main text.

be equally distributed around the mean. An excess of negative spikes thus points to translocation events, even if event duration τ and magnitude I_p are close to the detection limit of the setup under given conditions. For the data set shown in Fig. 2, we found 8008 events with positive and 15069 events with negative polarity (4σ cutoff), corresponding to 7061 events formally assigned to DNA translocation (580 s recording time, $c_{\text{DNA}} = 3 \text{ nM}$) This corresponds to a translocation frequency of $4 \text{ events}\cdot\text{s}^{-1}\cdot\text{nM}^{-1}$, which is comparable to those reported in ref. 48.

This is also reflected in the τ - and I_p -histograms shown on the right in Fig. 2. The prominent, sharp peak feature at $\tau_{mp,1} = 9 \mu\text{s}$ and $I_{mp,1} = 63 \text{ pA}$, respectively, appears in both positive and negative polarity traces. These events represent random noise, presumably convoluted with the filter response. For negative polarity, however, the DNA translocation events appear as a second distribution at longer τ /higher I_p . Formally, we obtained $\tau_{mp,2} = 16 \mu\text{s}$ and $I_{mp} \approx 80\text{-}90 \text{ pA}$. The distribution of the latter is surprisingly wide, which we speculate could be related to the orientation of the (short) DNA during translocation.⁴⁹

For data recorded at $V_{\text{bias}} = -100 \text{ mV}$ and -200 mV (not shown), we obtained for the DNA translocation events $\tau_{mp,2} = 22 \mu\text{s}$ and $20 \mu\text{s}$, respectively. While there seems to be a small increase in translocation time with decreasing V_{bias} , the small change suggests some filter convolution (filter frequencies were 50 and 60 kHz, respectively).

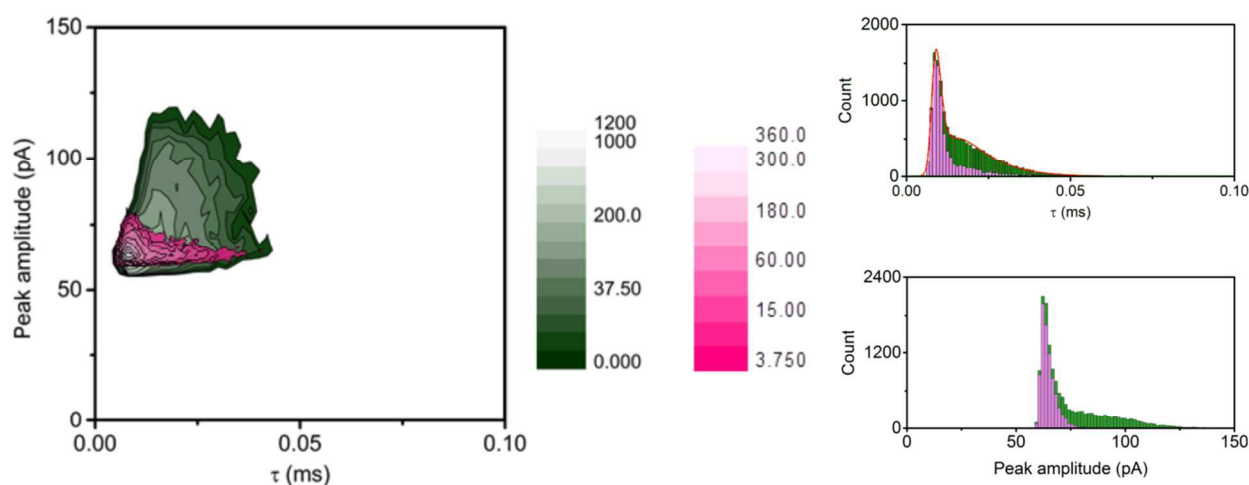


Fig. 2: Translocation of 200 bp dsDNA in 1 M KCl at $V_{\text{bias}} = -300 \text{ mV}$, filter frequency: 70 kHz. Green (magenta): Events with negative (positive) polarity. Left: Contour plots for each data set, I_p vs. τ . Right top/bottom: τ - and I_p - histograms. A double log-normal distribution fit (red line) is

included for the τ -histogram at negative event polarity (distribution 1: $\tau_{mean,1} = 9 \mu\text{s}$, $\tau_{mode,1} = \tau_{mp,1} = 9 \mu\text{s}$, std. dev. = 0.159; distribution 2: $\tau_{mean,2} = 19 \mu\text{s}$, $\tau_{mode,2} = \tau_{mp,2} = 16 \mu\text{s}$, std. dev. = 0.453). Pore conductance: 31 nS, estimated pore diameter, acc. to eq. (1): 17 nm. See further discussion in the main text.

In an effort to slow down the translocation process, we changed the electrolyte from 1 M KCl to 2 and 4 M LiCl, respectively, which has previously been shown to increase the translocation time by up a factor of 10.^{45,46} This has been rationalized in part by differences in ion pairing between K^+ and Li^+ and the DNA backbone. Interestingly, Bell et al. have recently shown that the change in electrolyte can also have more subtle consequences, such as a transition from flux- to barrier-limited translocation.⁴⁸

In any case, we were able to reproduce the qualitative trend of slowed translocation in highly concentrated LiCl electrolytes also for short dsDNA in nanopipettes. Translocation data for 100 bp DNA in 2 M LiCl electrolyte are shown in Fig. 3, at $V_{bias} = -100 \text{ mV}$ (left, blue; 40 kHz filter frequency, 5σ cutoff) and -200 mV (right, purple; 50 kHz filter frequency, 5σ cutoff). Both contour plots (top) show a single population of translocation events and no significant additional noise features. Accordingly, we did not observe any indication of different folding states of the DNA, which is unsurprising given their short length, in comparison with the persistence length. The τ -histogram is represented very well by a single log-normal distribution with maxima at $\tau_{mp} = 79 \mu\text{s}$ for $V_{bias} = -100 \text{ mV}$ and $\tau_{mp} = 46 \mu\text{s}$ for $V_{bias} = -200 \text{ mV}$, respectively. While the amount of data is clearly too limited for a systematic analysis of the bias dependence, we note that these values are roughly in-line with the V_{bias}^{-1} -dependence of τ_{mp} reported previously for translocation of long DNA in nanopipettes (see reference 42 and references therein). As above, the I_p -histogram is relatively broad and does not feature a distinct maximum (even though the contour plot does show a distinct event cluster, *vide supra*). The most probable I_p values are between 30 and 40 pA and appear to be higher for larger V_{bias} , as expected.

Kowalczyk et al. have previously quantified the increase in translocation time for long DNA upon changing the electrolyte from 1 M KCl to 1 M LiCl and 2 M LiCl with a chip-based nanopore.⁴⁵ They found a combined effect of $4.8 \cdot 1.5 = 7.2$, relative to the translocation time in 1 M KCl. Assuming a similar increase here, we estimate the τ_{mp} values for 100 bp dsDNA in 1 M KCl to be approximately 11 and 6 μs at $V_{bias} = -100 \text{ mV}$ and -200 mV , which would explain why this short

fragment remained undetected. Correspondingly, we would expect $\tau_{mp} \approx 22$ and $12 \mu\text{s}$ for 200 bp DNA at these bias voltages, which is similar to the experimental values obtained for this sample in 1M KCl, see above.

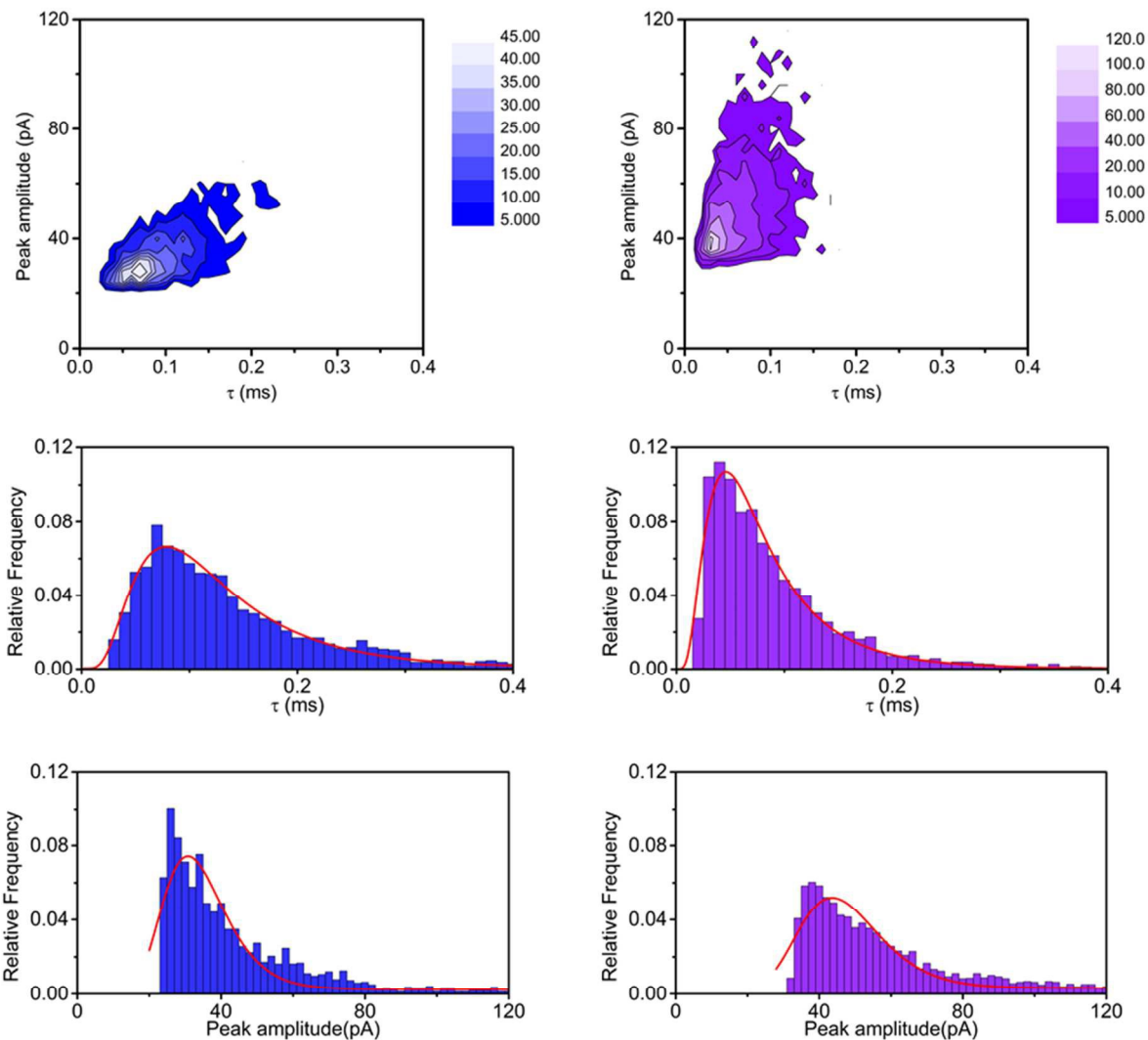


Fig. 3: Translocation experiments with 100 bp dsDNA in 2 M LiCl electrolyte, at $V_{bias} = -100$ mV (left, blue; 1650 events) and -200 mV (right, purple; 1682 events). Contour plot of I_p vs. τ (top); τ - (middle) and I_p -histogram (bottom), including log-normal distribution fits (red, solid lines). Filter frequency: 40 kHz ($V_{bias} = -100$ mV) and 50 kHz ($V_{bias} = -200$ mV), respectively. Pore conductance: 27 nS, estimated pore diameter: 22 nm.

A further increase in the translocation time of approximately 33% was observed upon increasing the LiCl concentration to 4 M.⁴⁵ While a direct comparison with the above data is complicated by device-to-device variation (i.e. the data was measured with different pipettes), we observed similar or slightly increased τ_{mp} values under these conditions. For $V_{bias} = -100$ mV, we found $\tau_{mp} = 85 \pm 9$ μ s and for $V_{bias} = -200$ mV, $\tau_{mp} = 42 \pm 2$ μ s (averages of 3). The bias dependence of τ_{mp} again appears to be in-line with the V_{bias}^{-1} dependence observed previously (*vide supra*), with τ_{mp} halved as V_{bias} is doubled.

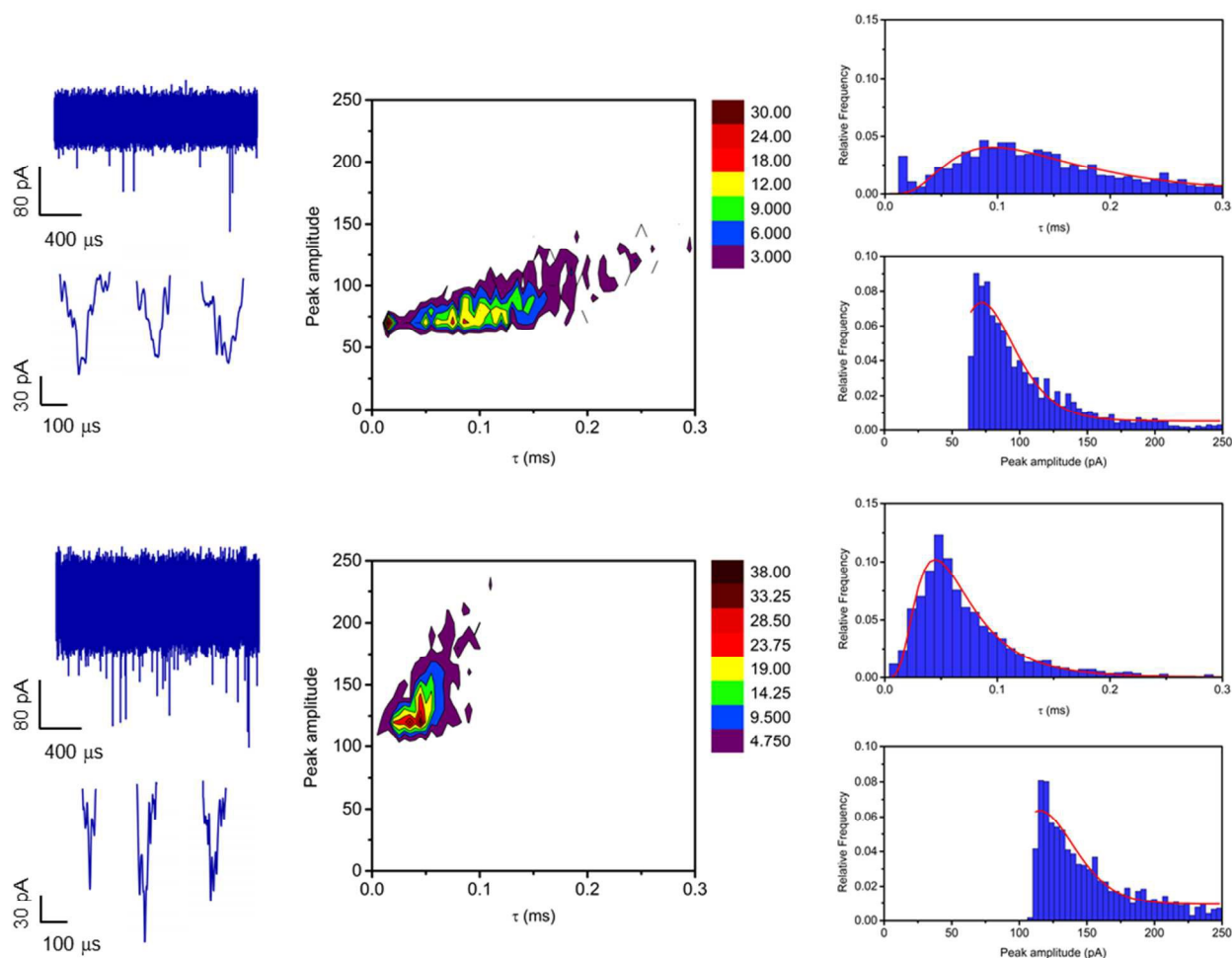


Fig. 4: Translocation experiments with 100 bp dsDNA in 4 M LiCl electrolyte, at $V_{bias} = -100$ mV (top, 2150 events) and -200 mV (bottom, 4012 events). Left: Sections of $I(t)$ traces in the presence of DNA in solution; translocation events are downward spikes. Middle: Contour plots of I_p vs. τ . Right: τ - and I_p -histograms, including log-normal distribution fits (red, solid lines). Filter frequency:

50 kHz ($V_{bias} = -100$ mV) and 100 kHz ($V_{bias} = -200$ mV), respectively. Pore conductance: 43 nS, estimated pore diameter: 21 nm.

In conclusion, we have presented a new electronics design for the high-bandwidth/low-current detection of translocation events in quartz nanopipettes with pore diameters in the region of 20 nm. In comparison to our previous work, this design features on-board voltage generation, triggered bias reversal and 'zapping' capabilities and software with fully integrated data acquisition and instrument control. Building on this work, we first theoretically assess and then demonstrate detection of 200 bp dsDNA in 1M KCl. The translocation time is on the order of 20 μ s or shorter and thus at the limit of detection. Upon changing the electrolyte from KCl to LiCl and increasing its concentration from 1 to 2 and 4 M, respectively, we slow down the translocation process (τ_{mp} between 50 and 100 μ s, depending on V_{bias}) and show that the detection of 100 bp dsDNA, and potentially even shorter fragments, is feasible with pores in this size range. A further slowing down of the process may be achieved using surface functionalization, *e.g.* silanization,⁴⁷ which we will explore in future work. Preliminary results for long DNA indeed show the expected effect (*cf.* SI), which also highlights the important role of DNA/surface interactions before or during the translocation process.⁴² In addition, an increase in the S/N ratio may be achieved with a reduction of the pore diameter.

While resolving features at the level of individual DNA bases (or base pairs) is beyond reach, and not the immediate aim of our work, the label-free detection of DNA fragments in 100 bp range may offer interesting prospects for disease detection and biomedical sensing, especially when coupled with suitable sampling processing.

References

- ¹ C. A. T. Chansin, R. Mulero, J. Hong, M.J. Kim, A.J. deMello, J.B. Edel, *Nano Lett.* 2007, 7, 2901-2906.
- ² M.P. Cecchini, A. Wiener, V.A. Turek, H. Chon, S. Lee, A.P. Ivanov, D.W. McComb, J. Choo, T. Albrecht, S.A. Maier, J.B. Edel, *Nano Lett.* 2013, 13, 4602-4609.
- ³ J.J. Kasianowicz, E. Brandin, D. Branton, D.W. Deamer, *Proc. Natl. Acad. Sci. USA* 1996, 93, 13770-13773.
- ⁴ J. Li, D. Stein, C. McMullan, D. Branton, M.J. Aziz, J.A. Golovchenko, *Nature* 2001, 412, 166-169.
- ⁵ A.P. Ivanov, E. Instuli, C.M. McGilvery, G. Baldwin, D.W. McComb, T. Albrecht, J.B. Edel, *Nano Lett.* 2011, 11, 279-285.
- ⁶ D. Fologea, M. Gershow, B. Ledden, D.S. McNabb, J.A. Golovchenko, J. Li, *Nano Lett.* 2005, 5, 1905-1909.
- ⁷ L.J. Steinbock, O. Otto, C. Chimere, J. Gornall, U.F. Keyser, *Nano Lett.* 2010, 10, 2493-2497.
- ⁸ D. Branton et al., *Nat. Biotechnol.* 2008, 26, 1146-1153.
- ⁹ J. Quick et al., *Nature* 2016, 530, 228-232.
- ¹⁰ A.R. Hall, A. Scott, D. Rotem, K.K. Mehta, H. Bayley, C. Dekker, *Nat. Nanotechnol.* 2010, 5, 874-877.
- ¹¹ E.C. Yusko, J.M. Johnson, S. Majd, P. Prangkio, R.C. Rollings, J. Li, J. Yang, M. Mayer, *Nat. Nanotechnol.* 2011, 6, 253-260.
- ¹² N.A.W. Bell, C.R. Engst, M. Ablay, G. Divitini, C. Ducati, T. Liedl, U.F. Keyser, *Nano Lett.* 2012, 12, 512-517.
- ¹³ A.J. Storm, J.H. Chen, X.S. Ling, H.W. Zandbergen, C. Dekker, *Nat. Mater.* 2003, 2, 537-541.
- ¹⁴ G.F. Schneider, S.W. Kowalczyk, V.E. Calado, G. Pandraud, H.W. Zandbergen, L.M.K. Vandersypen, C. Dekker, *Nano Lett.* 2010, 10, 3163-3167.
- ¹⁵ K. Liu, J. Feng, A. Kis, A. Radenovic, *ACS Nano* 2014, 8, 2504-2511.
- ¹⁶ D. Japrun, A. Bahrami, A. Nadzeyka, L. Peto, S. Bauerdick, J.B. Edel, T. Albrecht, *J. Phys. Chem. B* 2014, 118, 11605-11612.
- ¹⁷ A. Balan, B. Machielse, D. Niedzwiecki, J. Lin, P. Ong, R. Engelke, K.L. Shepard, M. Drndić, *Nano Lett.* 2014, 14, 7215-7220.
- ¹⁸ A. Balan, C.-C. Chien, R. Engelke, M. Drndić, *Sci Rep.* 2015, 5, 17775.
- ¹⁹ M.-H. Lee, A. Kumar, K.-B. Park, S.-Y. Cho, H.-M. Kim, M.-C. Lim, Y.-R. Kim, K.-B. Kim, *Sci. Rep.* 2014, 4, 7448.
- ²⁰ E. Neher, B. Sakmann, *Nature* 1976, 260, 799-802
- ²¹ B. Sakmann, E. Neher, *Ann. Rev. Physiol.* 1984, 46, 455-472.
- ²² P.K. Hansma, B. Drake, O. Marti, SAC Gould, CB Prater, *Science* 1989, 243, 641-643.
- ²³ C.-C. Chen, Y. Zhou, L.A. Baker, *Annu. Rev. Anal. Chem.* 2012, 5, 207-228.
- ²⁴ L.J. Steinbock, S. Krishnan, R.D. Bulushev, S. Borgeaud, M. Blokesch, L. Feletti, A. Radenovic, *Nanoscale* 2014, 6, 14380-14387.
- ²⁵ T.R. Gibb, A.P. Ivanov, J.B. Edel, T. Albrecht, *Anal. Chem.* 2014, 86, 1864-1871.
- ²⁶ J.Y.Y. Sze, S. Kumar, A.P. Ivanov, S.H. Oh, J.B. Edel, *Analyst* 2015, 140, 4828-4834.
- ²⁷ W.-J. Lan, D.A. Holden, B. Zhang, H.S. White, *Anal. Chem.* 2011, 83, 3840-3847.
- ²⁸ P.J. Hagerman, *Ann. Rev. Biophys. Biophys. Chem.* 1988, 17, 265-86.
- ²⁹ S. Brinkers, H.R.C. Dietrich, F.H. de Groote, I.T. Young, B. Rieger, *J. Chem. Phys.* 2009, 130, 215105.
- ³⁰ E.M. LeProust, B.J. Peck, K. Spirin, H. Brummel McCuen, B. Moore, E. Namsaraev, M.H. Caruthers, *Nucleic Acids Res.* 2010, 38, 2522-2540.
- ³¹ L.J. Steinbock, A. Lucas, O. Otto, U.F. Keyser, *Electrophoresis* 2012, 33, 3480-3487.
- ³² P. Nuttall, K. Lee, P. Ciccarella, M. Carminati, G. Ferrari, K.-B. Kim, T. Albrecht, *J. Phys. Chem. B*, 2016, 120, 2106-2114.
- ³³ T. Albrecht, M. Carminati, G. Ferrari, P. Nuttall, W. Pitchford and A. J. Rutkowska, "Electrochemical applications of nanopore systems" in *Electrochemistry, Volume 12: Nanosystems Electrochemistry*, Royal Chemical Society 2014, 155-186, ISBN 9781849735810, 2014.
- ³⁴ M. Carminati, G. Ferrari, A. P. Ivanov, T. Albrecht, M. Sampietro, *Analog Integr. Circ. Sig. Process.* 2013, 77, 3, 333-343.
- ³⁵ M. Carminati, M. Vergani, G. Ferrari, L. Caranzi, M. Caironi, M. Sampietro, *Sens. Actuators B* 2012, 174, 168-175.
- ³⁶ M. H. Lee, A. Kumar, K.B. Park, S.Y. Cho, H.M. Kim, M.C. Lim, Y.R. Kim and K.B. Kim, *Sci. Rep.* 2014, 4, 7448.
- ³⁷ A. Balan, C.-C. Chien, R. Engelke, M. Drndić, *Sci. Rep.* 2015, 5, 17775.
- ³⁸ J.K. Rosenstein, M. Wanunu, C.A. Merchant, M. Drndić, K.L. Shepard, *Nat. Methods* 2012, 9, 487-489.

-
- ³⁹ M. Crescentini, M. Bennati, M. Carminati, M. Tartagni, *IEEE Trans. Biomed. Circuits and Systems* 2014, 8, 2, 278-292.
- ⁴⁰ J. Larkin, R.Y. Henley, M. Muthukumar, J.K. Rosenstein, M. Wanunu, *Biophysical Journal* 2014, 106, 696-704.
- ⁴¹ P. Ciccarella, M. Carminati, G. Ferrari, R. Fraccari, A. Bahrami, *Proc. IEEE PRIME*, 2014, DOI: 10.1109/PRIME.2014.6872701.
- ⁴² R. L. Fraccari, P. Ciccarella, A. Bahrami, M. Carminati, G. Ferrari and T. Albrecht, *Nanoscale* 2016, 8, 7604-7611.
- ⁴³ J. Gershow, Marc; Golovchenko, *Nat. Nanotechnol.* 2007, 2, 775-779.
- ⁴⁴ C. Plesa, L. Cornelissen, M. W. Tuijtel, C. Dekker, *Nanotechnology* 2013, 24, 475101.
- ⁴⁵ S.W. Kowalczyk, D.B. Wells, A. Aksimentiev, C. Dekker, *Nano Lett.* 2012, 12, 1038-1044.
- ⁴⁶ J. Uplinger, B. Thomas, R. Rollings, D. Fologea, D. McNabb, J. Li, *Electrophoresis* 2012, 33, 3448–3457.
- ⁴⁷ Y.-R. Kim, J. Min, I.-H. Lee, S. Kim, A.-G. Kim, K. Kim, K. Namkoong, C. Ko, *Biosensors and Bioelectronics* 2007, 22, 2926-2931.
- ⁴⁸ N.A.W. Bell, M. Muthukumar, U.F. Keyser, *Phys. Rev. E* 2016, 93, 022401
- ⁴⁹ Y. Qiu et al., *ACS Nano* 2015, 9, 4390-4397.